Progress In Electromagnetics Research, PIER 76, 381–395, 2007

BISTATIC SCATTERING FROM THREE-DIMENSIONAL CONDUCTING ROUGH SURFACE WITH UV MULTILEVEL PARTITIONING METHOD

Z.-X. Li

Electromagnetic Academy
Zhejiang University
Hangzhou, Zhejiang, 310075, China

Abstract—Vector wave three-dimensional (3-D) conducting rough surface scattering problem solved by a **UV** method with multilevel partitioning (**UV-MLP**) is developed in this paper. For a 3-D conducting rough surface scattering problem, the scattering structure is partitioned into multilevel block. By looking up the rank in the static problem, the impedance matrix for a given transmitting and receiving block is expressed into a product of **U** and **V** matrix. The **UV** method is illustrated by applying to a 3D scattering problem of random conducting rough surface in this paper. Numerical simulation results are illustrated.

1. INTRODUCTION

Monte Carlo simulation of wave scattering from random rough surface problem have become an attractive approach recently, the prob-lem of scattering from rough surface has been studied with an-alytical solution [1–3]. Since modern computers technology and fast numerical methods have greatly been developed. The method of moment (**MoM**) has been used in numerical simulation to solve the surface integral equation method [4–11]. Conventional implementation of the MoM requires an $O(N^3)$ operation and an $O(N^2)$ computer memory storage. Two fast numerical methods have been used and they are the sparse matrix canonical grid method (SMCG) [7–10] and the Fast Multipole Method (FMM) [11]. Both methods have been applied to perfect electric conducting (PEC) and dielectric rough surfaces.

Recently, the **UV-MLP** is proposed to solve scalar wave scattering from the PEC rough surface problem in [12, 13] and dielectric rough surface problem in [14], the **UV-MLP** method has

achieved $O(N\log(N))$ based on the interpolation technique. The **UV-MLP** has been used to solve the volume scattering problem in [15].

In this paper, the **UV-MLP** method is developed to solve vector wave scattering from 3-D conducting rough surface problem. In the method, the impedance matrix was first be divided into four small matrices, then the multilevel partitioning (**MLP**) has been used to partition the each small impedance matrix. The surface area of the rough surface when projected onto the xy plane has a surface area up to $8\times 8 = 64$ square wavelengths with the number of surface unknowns of 8192. In this case, the **MLP** used is as done in the multilevel FMM.

The paper is organized as follows. In Section 2.1, the formulation of the problem of vector elec-tromagnetic wave impinging upon a 3-D conducting rough surface is given in magnetic field integral equation (MFIE), which is converted into a ma-trix equation using the MoM. In Section 2.2, the conducting rough sur-face problem independent rank determination is discussed. In Section 2.3, the MLP is described and in Section 2.4, the UV method is described. In Section 2.5, the computational complexity of the proposed algorithm is derived. In Section 3, numerical results are illustrated and discussed. Conclusions are given in Section 4.

2. METHODOLOGY

2.1. Formulation of Vector Wave Scattering from Conducting Rough Surface

Consider an electromagnetic wave $\bar{H}^i(x,y,z)$, with a time dependence of $e^{-i\omega t}$ impinging upon a 3-D conducting rough surface with a random height profile $z = f(x,y)$. It is tapered so that the illuminated rough surface can be confined to the surface area $L_x \times L_y$ [8]. The direction of incident wave is $\hat{k}_i = \sin\theta_i\cos\phi_i\hat{x} + \sin\theta_i\sin\phi_i\hat{y} - \cos\theta_i\hat{z}$. The incident fields are given as

$$\bar{H}^i(x,y,z) = -\frac{1}{\eta}\int_{-\infty}^{+\infty} dk_x \int_{-\infty}^{+\infty} dk_y \cdot e^{ik_x x + ik_y y - ik_z z} \tag{1}$$

$$\Psi(k_x,k_y)\cdot\hat{h}(-k_z) \tag{2}$$

where

$$\hat{e}(-k_z) = \frac{1}{k_\rho}(\hat{x}k_y - \hat{y}k_x) \tag{3}$$

$$\hat{h}(-k_z) = \frac{k_z}{kk_\rho}(\hat{x}k_x - \hat{y}k_y) + \frac{k_\rho}{k}\hat{z} \tag{4}$$

with $k_z = \sqrt{k^2 - k_x^2 - k_y^2}$, $k_\rho = \sqrt{k_x^2 + k_y^2}$. In above, k and η are wavenumber and wave impedance of free space, respectively. The spectrum of the incident wave $E(k_x, k_y)$ is given as

$$\Psi(k_x, k_y) = \frac{g^2}{4\pi} e^{\left[-g^2 \frac{(k_x - k_{ix})^2 + \left(k_y - k_{iy}\right)^2}{4}\right]} \tag{5}$$

The parameter g control the tapering of the incident wave and is set to $L_x/2 = L_y/2$ in the simulations of this paper. However, in (5), a spectrum of vector plane waves is used so that the incident wave obeys Maxwell's equations exactly.

The 3-D random conducting rough surface and with random height profile $z = f(x, y)$. The height function $z = f(x, y)$ has zero mean. Let $\bar{r}' = \hat{x}x' + \hat{y}y' + \hat{z}f(x', y')$ denote a source point and $\bar{r} = \hat{x}x + \hat{y}y + \hat{z}f(x, y)$ denote a field point on the rough surface. Then the MFIE on the perfectly conducting rough surface for $\bar{r}$ and $\bar{r'}$ on the surface is [16]

$$\hat{n} \times \bar{H}(\bar{r}) = 2\hat{n} \times \bar{H}^i(\bar{r}) + 2\hat{n} \times \iint_{S'} \nabla g \times \hat{n'} \times \bar{H}(\bar{r'}) ds' \tag{6}$$

where $\int\int_S$ denote a principal-integral.

$$\nabla g = (\bar{r} - \bar{r'}) G(R) \tag{7}$$

$$G(R) = \frac{(ikR - 1)e^{ikR}}{4\pi R^3} \tag{8}$$

and $R = |\bar{r} - \bar{r'}| = \sqrt{(x - x')^2 + (y - y')^2 + (z - z')^2}$

The **MoM** is used to discretize the integral equation. We use the pulse basis function and point-matching method. Recasting the MFIE into scalar form and in terms of I_x and I_y components, we have

$$\begin{aligned} I_x^i = {} & \frac{I_x}{2} + \int_{S'} \left(f_y(y - y') + f_{x'}(x - x') - (z - z')\right) G(r, r') I_{x'} dS' \\ & - \int_{S'} (f_y(x - x') - f_{y'}(x - x')) G(r, r') I_{y'} dS' \end{aligned} \tag{9}$$

$$\begin{aligned} I_y^i = {} & - \int_{S'} (f_x(y - y') - f_{x'}(y - y')) G(r, r') I_{x'} dS' \\ & + \frac{I_y}{2} + \int_{S'} \left(f_x(x - x') + f_{y'}(y - y') - (z - z')\right) G(r, r') I_{y'} dS' \end{aligned} \tag{10}$$

so we write the scalar equations into matrix form

$$\bar{\bar{Z}} \cdot \bar{I} = \bar{I}^i \tag{11}$$

where $\bar{I} = [I_{x'}, I_{y'}]^{-1}$, $\bar{I}^i = \left[I_x^i, I_y^i\right]^{-1}$ and

$$I_{x'}(\bar{r}) = \sqrt{1 + f_{x'}^2 + f_{y'}^2}\hat{n'} \times \bar{H}(\bar{r'}) \cdot \hat{x} \tag{12}$$

$$I_{y'}(\bar{r'}) = \sqrt{1 + f_{x'}^2 + f_{y'}^2}\hat{n'} \times \bar{H}(\bar{r'}) \cdot \hat{y} \tag{13}$$

$$I_x^i(\bar{r}) = \hat{n} \times \bar{H}^i(\bar{r}) \cdot \hat{x} \tag{14}$$

$$I_y^i(\bar{r}) = \hat{n} \times \bar{H}^i(\bar{r}) \cdot \hat{y} \tag{15}$$

The impedance matrix $\bar{\bar{Z}}$ can be further divided into four matrices ($\bar{\bar{Z}}_{11}$, $\bar{\bar{Z}}_{12}$, $\bar{\bar{Z}}_{21}$, $\bar{\bar{Z}}_{22}$), which has been given in Fig. 1.

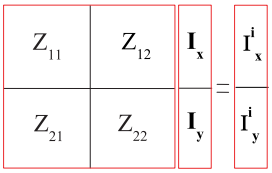

Figure 1. Illustration of impedance matrix partitioning process.

2.2. Rank Determination for Conducting Random Rough Surface

For the 3-D conducting rough surface scattering problem, the difficulty is that the vertical sizes of the blocks are always changed due to the randomness of surface height. Thus the coarse-coarse are sampling have to be used to determine the rank. In the simulation, 16 points per square wavelength (instead of 100 points per square wavelength) are used for rank determination. In Table 1, the conducting rough surface area is $8\lambda \times 8\lambda$, the ranks as functions of the rms δ, correlation length ℓ and distance d between two interaction groups are shown. The results are obtained through one realization of rough surface profile with the given varied rms height of 0.01λ, 0.05λ, and 0.10λ, varied correlation length of 0.707λ, 1.414λ and 2.0λ.

Table 1 shows that ranks of $\overline{\overline{Z}}_{11}$, $\overline{\overline{Z}}_{12}$, $\overline{\overline{Z}}_{21}$, $\overline{\overline{Z}}_{22}$, which are slowly varied with the correlation length ℓ and rms δ of conducting rough surface. From the table, we can see that maximum value of rank is associated with the nearest distance d between two group elements, on the other hand, minimum rank is associated with the remotest distance d between two group elements.

The minimum value of ranks of both $\overline{\overline{Z}}_{11}$, $\overline{\overline{Z}}_{12}$ and $\overline{\overline{Z}}_{21}$ is 4, which are independent on the rms δ and correlation length ℓ. The minimum

Table 1. rank table for variation of rms δ and correlation length of conducting rough surface.

		$\overline{\overline{Z}}_{11}$		$\overline{\overline{Z}}_{12}$		$\overline{\overline{Z}}_{21}$		$\overline{\overline{Z}}_{22}$	
$\delta(\lambda)$	$\ell(\lambda)$	1*	2*	1	2	1	2	1	2
0.01	0.707	24	4	24	4	24	4	24	4
	1.414	25	4	25	4	24	4	24	3
	2.000	23	4	23	4	23	4	22	4
0.05	0.707	29	4	31	4	29	4	28	4
	1.414	25	4	25	4	24	4	24	3
	2.000	23	4	23	4	23	4	22	4
0.10	0.707	30	4	34	4	33	4	30	4
	1.414	25	4	27	4	26	4	24	4
	2.000	23	4	24	4	24	4	23	4

1 * Maximum value of ranks;

2 * Minimum value of ranks;

value of ranks of $\overline{\overline{Z}}_{22}$ is 3-4 in Table 1, which is less dependent on the rms δ and correlation length ℓ variation.

The maximum value of ranks of $\overline{\overline{Z}}_{11}$, $\overline{\overline{Z}}_{12}$, $\overline{\overline{Z}}_{21}$ and $\overline{\overline{Z}}_{22}$ are dependent on rms δ when the correlation length ℓ is smaller, and become independent on the rms δ when the the correlation length ℓ is bigger. On the other hand, the maximum value of ranks of $\overline{\overline{Z}}_{11}$, $\overline{\overline{Z}}_{12}$, $\overline{\overline{Z}}_{21}$ and $\overline{\overline{Z}}_{22}$ are less dependent on the correlation length ℓ when rms δ is bigger, and become independent on correlation length ℓ when the rms δ become smaller.

In the SVD, the rank determination is based on a threshold. Thus there is built in variation of rank due to variations of threshold. Furthermore, in applications as illustrated in this paper, the exact rank is not required. Thus we usually are on the safe side, and use 10% to 20% above the "actual" rank.

We note that the selections of blocks are dependent on the type of problem. However, once the static rank table is determined, the rank table can be applied to all cases within the same type of problem.

2.3. Multi-level Partitioning Process

The impedance matrix of conducting rough surface can be divided into four small matrices ($\bar{\bar{Z}}_{11}$, $\bar{\bar{Z}}_{12}$, $\bar{\bar{Z}}_{21}$, $\bar{\bar{Z}}_{22}$), which can be seen in Fig. 1.

So each small matrix can used **UV-MLP** method to increase the code's efficiency. In order to sententious explain the **MLP**, for example, Z_{11} will be used below.

The **MLP** for the small $\bar{\bar{Z}}_{11}$ is same as the one in the case of 3D PEC rough surface scattering problem [13], which has been shown in Fig. 2.

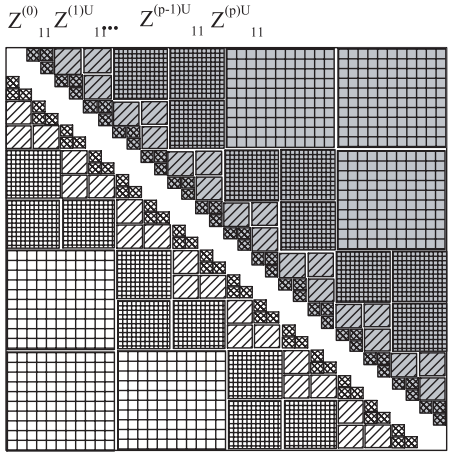

Figure 2. Illustration of impedance matrix partitioning process.

Since each of the four small matrices can be processed through **MLP** just like above, the **MLP** of impedance matrix consisted of four small matrices can be gotten, which can be shown in Fig. 3.

2.4. UV Method Based on Interpolation Technique

Since the impedance matrix has been divided into four small matrices ($\bar{\bar{Z}}_{11}$, $\bar{\bar{Z}}_{12}$, $\bar{\bar{Z}}_{21}$, $\bar{\bar{Z}}_{22}$), the **UV-MLP** method can be used to each small matrix. One of the four small matrices will be given to illuminate the **UV** method, for example, $\bar{\bar{Z}}_{11}$ will also be used.

$\bar{\bar{Z}}_{11}$ will be partitioned into multilevel block through **MLP**, which has been shown in Fig. 1. Every block except for the 0^{th} level is decomposed into matrix products. Consider a block $\bar{\bar{A}}$ of dimensional $N_0 \times N_0$, which represents the interactions of a transmitting group and a no-neighbor receiving group. We can use the **SVD** to determine the rank. Let σ_1 be the largest singular value and the singular value be arranged in decreasing magnitude. Given a threshold ϵ, the rank r is such that $\frac{\sigma_{r+1}}{\sigma_1} \leq \epsilon$.

If the size of the block $\bar{\bar{A}}$ becomes larger, it would consume CPU

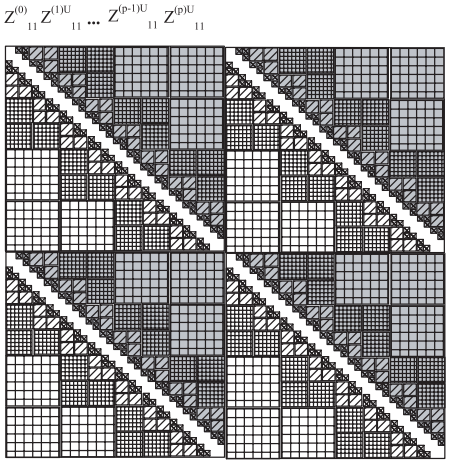

Figure 3. Illustration of impedance matrix partitioning process.

memory intensively. However, generally, the rank is much smaller than the size of the block. Thus, we can use coarse-coarse sampling for searching the rank. Namely, we uniformly pick the number of points in the transmitting group and a set of points in the received group, and form a new matrix of dimensions that are slightly larger than the rank, and we find the rank via the new matrix to be roughly same as that via the block $\bar{\bar{A}}$. This means we have a prior knowledge of roughly what is the rank, based on the numerical experiments carried out. As an exact rank is not required, in coarse sampling we can pick the number of points to be several times larger than the rank.

By looking up its rank r with the **SVD** and fast coarse-coarse sampling, the block $\bar{\bar{A}}$ is expressed as

$$\bar{\bar{A}}_{N_0 \times N_0} = \bar{\bar{U}}_{N_0 \times r} \bar{\bar{V}}_{r \times N_0} \tag{16}$$

where $\bar{\bar{V}}_{r \times N_0} = (\bar{\bar{\tilde{U}}}_{r \times r})^{-1} \bar{\bar{R}}_{r \times N_0}$ is calculated by LU decomposition using Crouts method with partial pivoting instead of an inversion of $\bar{\bar{\tilde{U}}}$. The column of $\bar{\bar{U}}$ are r columns of $\bar{\bar{A}}$ with uniform distribution, the rows of $\bar{\bar{R}}$ are r rows of $\bar{\bar{A}}$ with uniform distribution, and the rows of $\bar{\bar{\tilde{U}}}$ are r rows of $\bar{\bar{U}}$ with uniform distribution.

Generally, the rank of the block is much less than its dimension, so that in an iterative solution to the matrix equation, using matrices **U** and **V** instead of the block matrix to multiply with a vector, the computational time and memory requirement can be decreased from $O(N_o^2)$ to $O(2rN_0)$.

2.5. Computational Complexity Analysis

The impedance matric of conducting rough surface can be divided into four small matrices ($\bar{\bar{Z}}_{11}$, $\bar{\bar{Z}}_{12}$, $\bar{\bar{Z}}_{21}$, $\bar{\bar{Z}}_{22}$), which can be seen in Fig. 1. So each small matrix can be used **UV-MLP** method. In order to sententious analysis computational complexity of the **UV-MLP**, one of the four small matrices is first analyzed, for examples, $\bar{\bar{Z}}_{11}$ will be used.

2.5.1. Computational Complexity Analysis of the $\bar{\bar{Z}}_{11}$

The computational complexity analysis of the $\bar{\bar{Z}}_{11}$ is just same as the one in the case 3D PEC rough surface scattering [13]. The total computational steps for multilevel partitioning **UV** is sum of the near and non-near interactions of the $\bar{\bar{Z}}_{11}$ and is given by

$$27rN\log_2\left(\frac{N}{M_1}\right)+60rN-120rM_1+\left(9NM_1-12N^{\frac{1}{2}}\right)M_1^{\frac{3}{2}}+4M_1^2 \tag{17}$$

2.5.2. Computational Complexity Analysis of the $\bar{\bar{Z}}$

Since computational complexity analysis of one of the four small matrices ($\bar{\bar{Z}}_{11}$) has been finished above, so the total computational steps for multilevel **UV** to the matrix $\bar{\bar{Z}}$ consisted of four small matrices ($\bar{\bar{Z}}_{11}$, $\bar{\bar{Z}}_{12}$, $\bar{\bar{Z}}_{21}$, $\bar{\bar{Z}}_{22}$) is given by

$$4\times\left[27rN\log_2\left(\frac{N}{M_1}\right)+60rN-120rM_1+\left(9NM_1-12N^{\frac{1}{2}}\right)M_1^{\frac{3}{2}}+4M_1^2\right] \tag{18}$$

3. NUMERICAL RESULTS AND DISCUSS

The numerical simulation results will be presented in terms of the normalized bistatic cross section. For a scattered wave in α polarization and an incident wave in β polarization

$$\sigma^s_{\alpha\beta}(\theta_s,\phi_s)=\frac{4\pi|\bar{E}^s_\alpha|^2}{2\eta P_i} \tag{19}$$

where $\alpha = V$ or H, $\beta = V$ and the observation direction is $\hat{k}_s = \sin\theta_s\cos\phi_s\hat{x} + \sin\theta_s\sin\phi_s\hat{y} + \cos\theta_s\hat{z}$, the incident wave power is

$$P_i = \frac{2\pi^2}{\eta}\int_{k_\rho<k} dk_x dk_y \left(|E_V|^2\right)\frac{k_z}{k} \tag{20}$$

So $\sigma_{\alpha\beta}$ are, respectively

$$\sigma^s_{HV} = \frac{\eta ik}{4\pi}\int_{S'} dx'dy'e^{-ikr'}\cdot[-I_{x'}(x',y',z')\sin\phi_s + I_{y'}(x',y',z')\cos\phi_s] \tag{21}$$

and

$$\sigma^s_{VV} = \frac{\eta ik}{4\pi}\int_{S'} dx'dy'e^{-ikr'}\cdot[I_{x'}(x',y',z')\cos\theta_s\cos\phi_s + I_{y'}(x',y',z')$$
$$\cos\theta_s\sin\phi_s - (f_{x'}(x',y',z')I_{x'}(x',y',z') + f_{y'}(x',y',z')I_{y'}(x',y',z'))\sin\theta_s] \tag{22}$$

where $r' = x'\sin\theta_s\cos\phi_s + y'\sin\theta_s\sin\phi_s + f(x',y')\cos\theta_s$

Simulations are based on Gaussian random rough surfaces with Gaussian correlation functions.

Energy conservation check is essential. For a conducting rough surface, the reflectivity should be unity, which can be calculated in term of the surface fields.

$$r(\theta_i) = \frac{P_s}{P_i} = \frac{\int_{S'} ds\hat{n}\cdot\frac{1}{2}\mathrm{Re}\left[\bar{E}_s\times\bar{H}_s\right]}{P_i} \tag{23}$$

where $\bar{E}_s$ and $\bar{H}_s$ are the surface scattered fields.They are calculated as $\bar{E}_s = -\hat{n}\times\bar{E}_i$ and $\bar{H}_s = \bar{J} - \hat{n}\times\bar{H}_i$. The surface fields are calculated for each realization, and we can calculate reflectivity using Eq. (23). Then, we check whether $r(\theta_i)$ is equal to unity. In this paper, results of $r(\theta_i)$ is provided for the simulations.

3.1. Comparison between the UV and SVD

To show the validity of **UV** method, one realization for a conducting rough surface is used, whose parameters are given as: the rms height and correlation length of the rough surface are 0.05λ and 1.414λ, respectively. The surface lengths are 8 by 8 wavelengths and the incidence angle is 30 degrees. Both SVD and UV methods are utilized to calculate the bistatic scattering coefficient from the realization. Fig. 4 and Fig. 5 give the comparison bistatic scattering coefficients

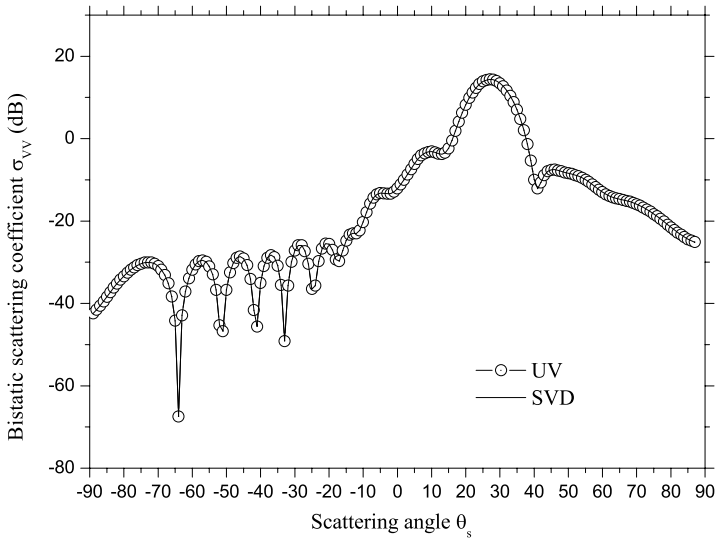

Figure 4. Comparison scattering coefficient σ_{VV} between **SVD** and **UV** methods.

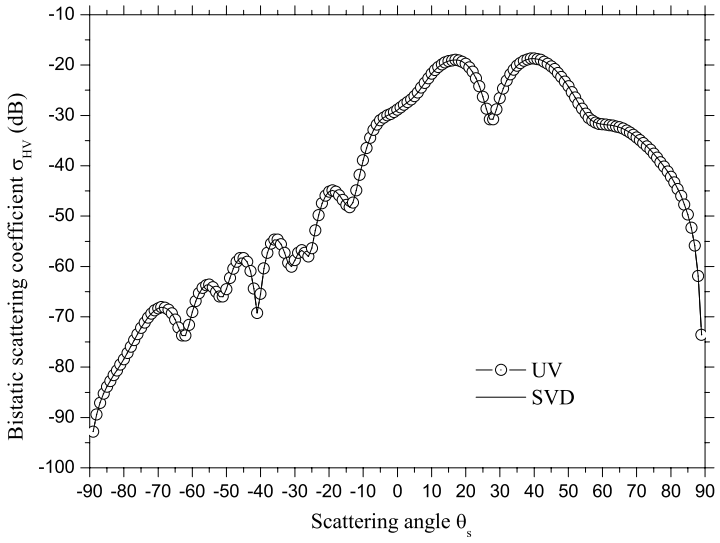

Figure 5. Comparison scattering coefficient σ_{HV} between **SVD** and **UV** methods.

σ_{VV} and σ_{HV} between **SVD** and **UV** methods and show the two curves are superposition. On the other hand, the energy conservation of the 3-D conducting rough surface is calculated through integral scattering coefficient over half above space, the reflectivity of the two method seem equal to each other (1.0002(UV), 1.0003(SVD)).

3.2. Analysis Distribution of the Induced Current

Figs. 6, 7 and 8 show the 3-D distribution of the induced current I_x, I_y and I_z. From the three figures, we can see that induced current I_x, I_y or I_z show the characteristic of tapered incident wave, the small amplitude of currents are around the edge of the conducting rough surface ($\delta = 0.10\lambda$, $\ell = 1.414\lambda$) illuminated with tapered incident wave.

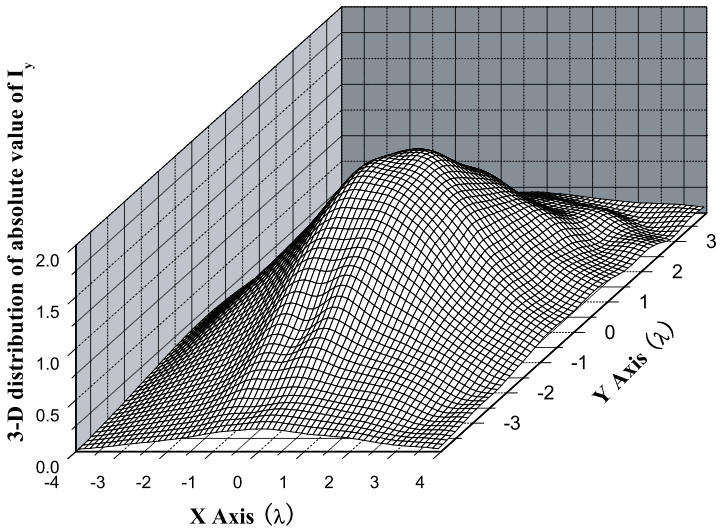

Figure 6. 3-D distribution of absolute value of induced current I_x.

3.3. Discuss of the Bistatic Scattering Coefficients Averaged over 30 Realizations.

In Fig. 9 and Fig. 10, we simulated the bistatic scattering coefficients σ_{VV} and σ_{HV} averaged over 30 realizations through the **UV** method. The rms height are 0.03λ, 0.05λ and 0.10λ, respectively, and all of their correlation length are 1.414λ. The surface lengths are 8 by 8 wavelengths and the incidence angle is 30 degrees. For VV case,

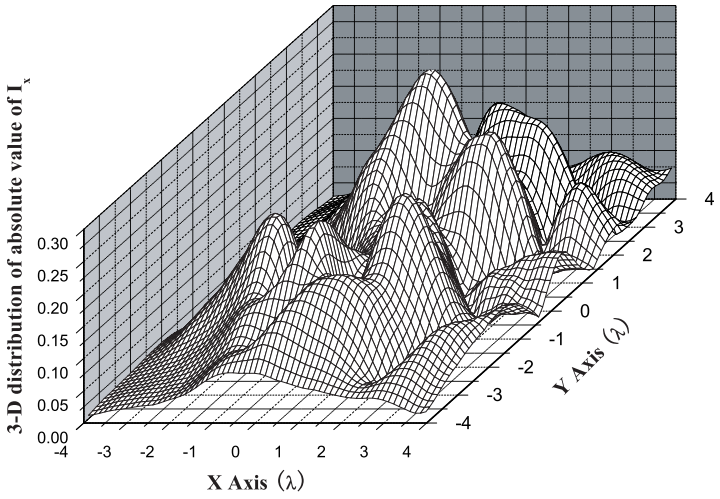

Figure 7. 3-D distribution of absolute value of induced current I_y.

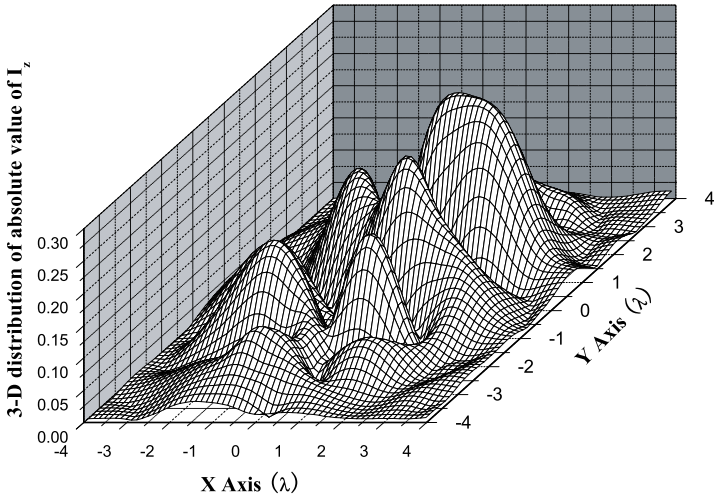

Figure 8. 3-D distribution of absolute value of induced current I_z.

the Fig. 9 shows that the the backscattering coefficient will increase with rms height increasing, on the contrary, the specular scattering coefficient will decrease, which opposites to the rms height's increasing. Meanwhile, for HV case, the Fig. 10 shows that the the backscattering coefficient will also increase with rms height increasing, so does the specular scattering coefficient, which opposites to the VV case.

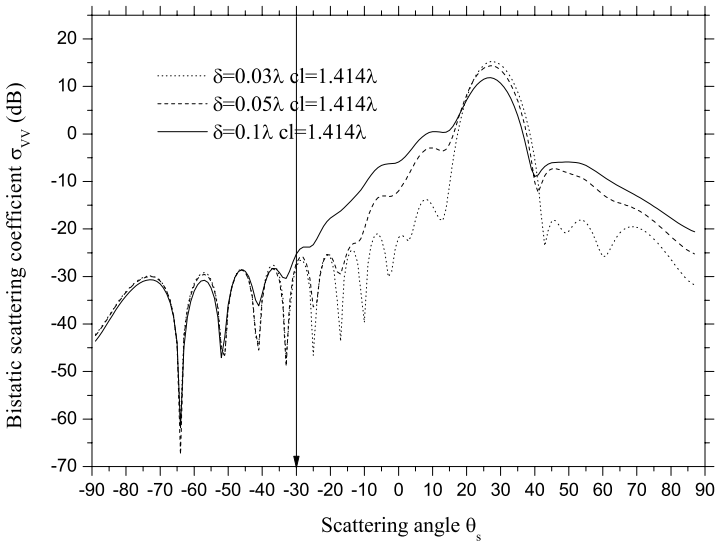

Figure 9. The bistatic scattering coefficients σ_{VV} averaged over 30 realizations.

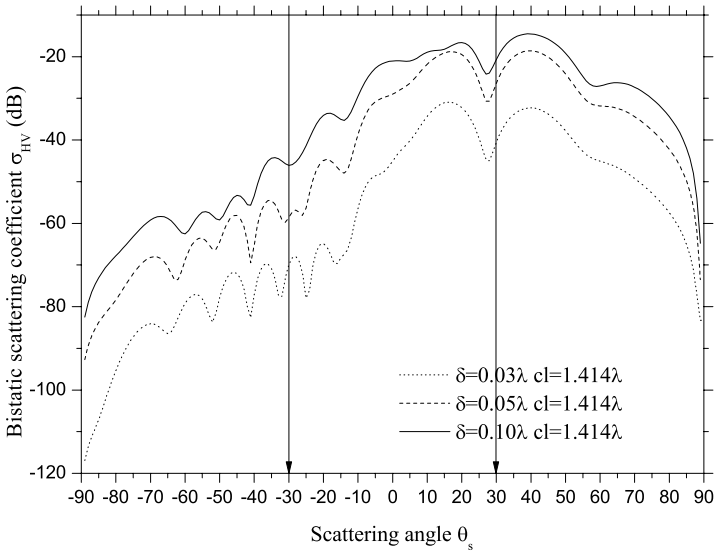

Figure 10. The bistatic scattering coefficients σ_{HV} averaged over 30 realizations.

4. CONCLUSION

In this paper, the **UV-MLP** method can be used for rapid solution of vector electromagnetic wave scattering from 3D PEC rough surface scattering. The method can be applied to 3D PEC rough surface scattering, and volume scattering of moderate size particles using high-order spherical wave Green's functions. Presently the case of vector electromagnetic wave scattering by lossy dielectric random rough surfaces are being studied.

ACKNOWLEDGMENT

The research in this paper was supported by the Innovation Fund of Space Flight Science and Technology, and the Electromagnetic Academy at Zhejiang University.

REFERENCES

1. Fung, A. K. and N. C. Kuo, "Backscattering from multi-scale and exponentially correlated surfaces," *J. of Electromagn. Waves and Appl.*, Vol. 20, No. 1, 3–11, 2006.
2. Chen, K. S., A. K. Fung, J. C. Shi, and H. W. Lee, "Interpretation of backscattering mechanisms from non-Gaussion correlated randomly rough surface," *J. of Electromagn. Waves and Appl.*, Vol. 20, No. 1, 105–118, 2006.
3. Hsieh, C.-Y. and A. K. Fung, "Depolarized upward and downward multiple scattering from a very rough surface," *Progress In Electromagnetics Research*, PIER 54, 199–220, 2005.
4. Maradudin, A. A., E. R. Mendez, and T. Michel, "Backscattering effects in the elastic scattering of p-polarization light from a large amplitude random grating," *Scattering in Volumes and Surfaces*, M. Nieto-Vesperians and J. C. Dainty (eds.), Elsevier Science Publishers, North-Holland, 1990.
5. Nieto-Vesperinas, M. and J. M. Soto-Crespo, "Monte-Carlo simulations for scattering of electromagnetic waves from perfectly conducting random rough surfaces," *Optics Letter*, Vol. 12, 979–981, 1987.
6. Chen, K. S., L. Tsang, and J. C. Shi, "Microwave mission from two-dimensional inhomogeneous dielectric rough surfaces based on physics-based two-grid method," *Progress In Electromagnetics Research*, PIER 67, 181–203, 2007.

7. Tsang, L., C. H. Chan, and K. Pak, "Backscattering enhancement of a two-dimensional random rough surface (three-dimensional scattering) based on Monte Carlo simulations," *Journal of Optical Society of America A*, Vol. 11, 711–715, 1994.
8. Pak, K., L. Tsang, and J. Johnson, "Numerical simulations and backscattering enhancement of electromagnetic waves from two-dimensional dielectric random rough surfaces with the sparse-matrix canonical grid method," *Journal of Optical Society of America A*, Vol. 14, No. 7, 1515–1529, July 1997.
9. Tsang, L., C. H. Chan, and K. Pak, "Monte Carlo simulation of a two-dimensional random rough surface using the sparse-matrix flat-surface iterative approach," *Electronic Letter*, Vol. 29, 1153–1154, 1993.
10. Pak, K., L. Tsang, C. H. Chan, and J. Johnson, "Backscattering enhancement of vector electromagnetic waves from two-dimensional perfectly conducting random rough surfaces based on Monte Carlo simulations," *Journal of Optics Society of America, A*, Vol. 12, 2491–2499, 1995.
11. Jandhyala, V., E. Michielssen, S. Balasubramaniam, and W. C. Chew, "A combined steepest descent-fast multipole algorithm for the fast analysis of three-dimensional scattering by rough surfaces," *IEEE Transactions on Geoscience Remote Sensing*, Vol. 36, 738–748, 1998.
12. Tsang, L., D. Chen, and P. Xu, "Wave scattering with the UV multilevel partitioning method: 1, two dimensional problem of perfect electric conductor surface scattering," *Radio Science*, Vol. 39, RS5010, 2004.
13. Tsang, L., Q Li, P. Xu, et al., "Wave scattering with the UV multilevel partitioning method: 2, three dimensional problem of nonpenerable surface scattering," *Radio Science*, Vol. 39, RS5010, 2004.
14. Li, Z. X., "Wave scattering with the UV multilevel partitioning method: three dimensional problem of dielectric rough surface scattering," *Microwave and Optical Technology Letter*, Vol. 48, 1313–1317, 2006.
15. Tsang, L. and Q. Li, "Wave scattering with the UV multilevel partitioning method for volume scattering by discrete scatters," *Microwave and Optical Technology Letter*, Vol. 12, 354–361, 2004.
16. Tsang, L., J. A. Kong, K. H. Ding, and C. O. Ao, *Scattering of Electromagnetic Waves*, Vol. 2: Numerical Simulations, Wiley Interscience, 2001.